Volume 16
Number 4
28 January 2020
Pages 845–1126

Soft Matter

rsc.li/soft-matter-journal

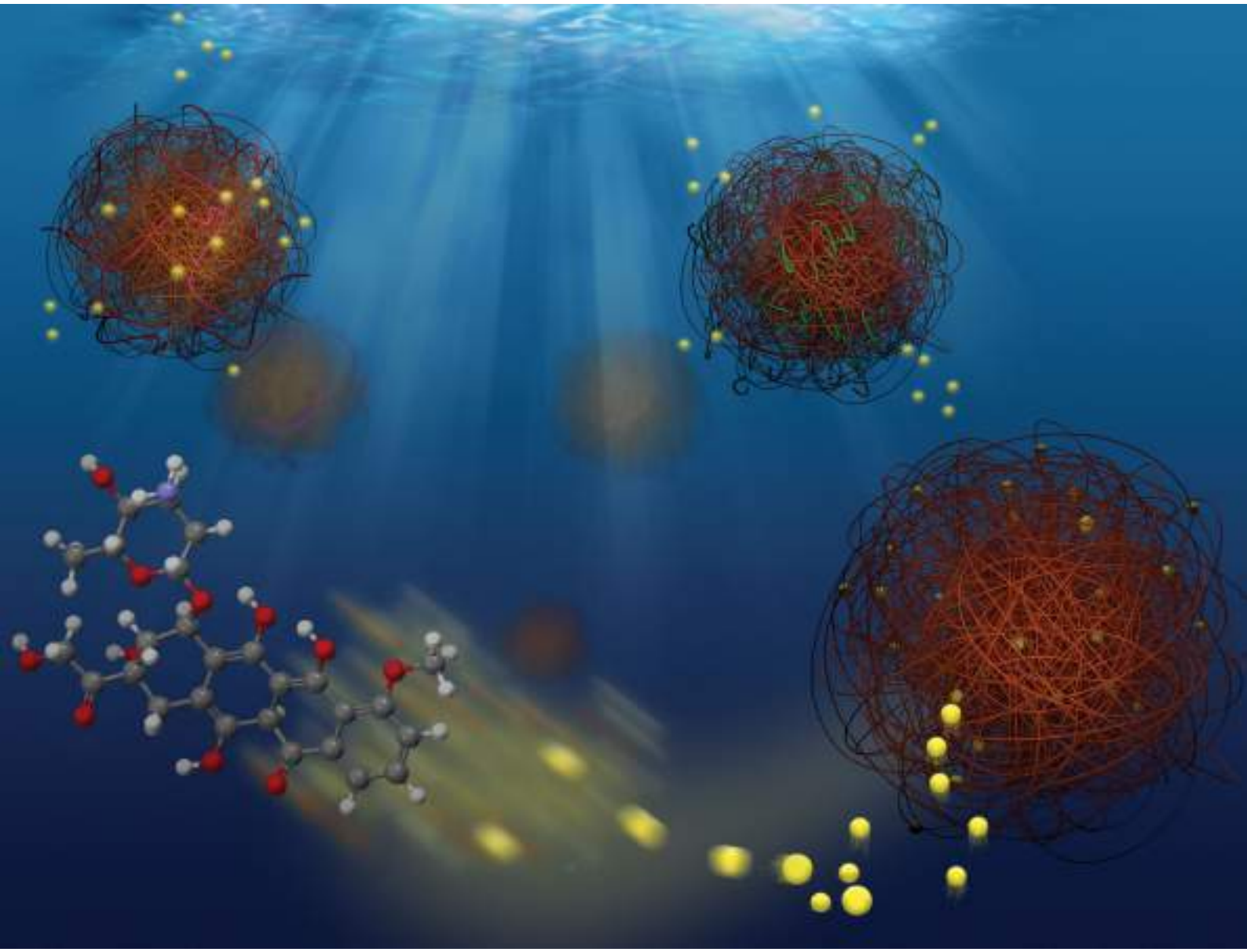

ISSN 1744-6848

ROYAL SOCIETY OF CHEMISTRY

PAPER

Juan M. Giussi, Sergio Moya *et al.*
A study of the complex interaction between poly allylamine hydrochloride and negatively charged poly(*N*-isopropylacrylamide-*co*-methacrylic acid) microgels

Soft Matter

PAPER

Cite this: *Soft Matter*, 2020, **16**, 881

A study of the complex interaction between poly allylamine hydrochloride and negatively charged poly(*N*-isopropylacrylamide-*co*-methacrylic acid) microgels†

Juan M. Giussi,[a]* Marta Martínez Moro,[b] Agustín Iborra,[a] M. Lorena Cortez,[a] Desiré Di Silvio,[b] Irantzu Llarena Conde,[b] Gabriel S. Longo,[a] Omar Azzaroni[a] and Sergio Moya[b]*

Negatively charged poly(*N*-isopropylacrylamide-*co*-methacrylic acid) (P(NIPAm-*co*-MAA)) microgels undergo size changes in response to changes in temperature and pH. Complexation of these microgels with positively charged polyelectrolytes can greatly affect their physical properties and their capacity for encapsulating active molecules. Here we study the interaction between (P(NIPAm-*co*-MAA)) microgels and a model positively charged polyelectrolyte, poly allylamine hydrochloride (PAH), with different molecular weights. Experiments were conducted at temperatures below and above the lower critical solution temperature (LCST) of the microgel (30–32 °C), at 20 and 40 °C, respectively, and for PAH at molecular weights of 15, 50, and 140 kDa. Below the LCST, dynamic light scattering and zeta potential measurements with molecular simulation show that for the 15 kDa PAH there is preferential accumulation of PAH inside the microgel, whereas for the higher molecular weight PAH, the polyelectrolyte deposits mainly on the microgel surface. Above the LCST, PAH is preferentially located on the surface of the microgels for all molecular weights studied as a result of charge segregation in the hydrogels. Confocal scanning laser microscopy and flow cytometry were used to quantify rhodamine labelled PAH associated with the microgel. Isothermal titration calorimetry studies give insight into the thermodynamics of the interaction of PAH with the hydrogels, and how this interaction is affected by the molecular weight of PAH. Finally, microgels with encapsulated doxorubicin were exposed to PAH, revealing that the drug is displaced from the microgel by the PAH chains.

Received 17th October 2019,
Accepted 21st December 2019

DOI: 10.1039/c9sm02070e

rsc.li/soft-matter-journal

Introduction

Micrometer-sized hydrogels, microgels, are highly-hydrated cross-linked polymer networks in the colloidal domain. Microgels are usually designed to undergo a volume phase transition in response to specific stimuli, such as temperature, pH, ionic strength, or solvent nature. Microgels based on poly(*N*-isopropylacrylamide) (PNIPAm) are probably the most studied thermosensitive hydrogels. PNIPAm hydrogels exhibit a volume phase transition at 30–32 °C, the so-called nominal lower critical solution temperature (LCST). Above this temperature, the cross-linked PNIPAm chains stabilized by hydrogen bonding with water dehydrate, resulting in a drastic particle size decrease. Microgels with temperature sensitivity near physiological conditions have drawn increasing attention due to their potential application in sensing,[1,2] regenerative medicine,[3] and drug delivery.[4,5]

PNIPAm based microgels, though practically not charged, are highly solvated in water by hydrogen bonding interactions and provide an environment suitable for hydrophilic and charged drugs. However, the encapsulation and retention of charged drugs in PNIPAm-based microgels is limited and it is necessary to increase the loading capacity of the microgel by introducing ionic co-monomers into the PNIPAm network that can trap oppositely charged molecules. Microgels based on PNIPAm and methacrylic acid (poly(*N*-isopropylacrylamide-*co*-methacrylic acid) (P(NIPAm-*co*-MAA))) are both thermoresponsive and pH-sensitive, while also being capable of complexing positively charged drugs through carboxylic groups. Besides drug delivery,[6,7] P(NIPAm-*co*-MAA) microgels are increasingly employed in emulsion stabilization,[8,9] thin-film fabrication,[10–12] gelling,[13]

[a] *Instituto de Investigaciones Fisicoquímicas Teoricas y Aplicadas (INIFTA), Departamento de Química, Facultad de Ciencias Exactas, Universidad Nacional de La Plata, CONICET, 1900 La Plata, Argentina. E-mail: jmgiussi@inifta.unlp.edu.ar*

[b] *Soft Matter Nanotechnology Group, CIC BiomaGUNE, Paseo Miramon 182, 20014, San Sebastian, Spain. E-mail: smoya@cicbiomagune.es*

† Electronic supplementary information (ESI) available. See DOI: 10.1039/c9sm02070e

and for nanomaterial templating,[14,15] among other applications. Moreover, the distribution of ionizable groups in the microgels (random and core–shell) controls the interactions for the uptake and release of certain guests.[16]

Charged thermoresponsive microgels can also be assembled into films using the Layer-by-Layer (LbL) technique, which expands their potential applications in sensing and delivery. In previous work, we have assembled P(NIPAm-*co*-MAA) microgels with poly allyl amine hydrochloride (PAH) as a counter polyelectrolyte. The microgel is alternatingly assembled with PAH up to a desired number of layers. Interestingly, we could observe that during their assembly the microgels decrease their water content.[17] However, the LbL films retain thermoresponsiveness from the microgels and exhibit an increase in hydrophobicity, stiffness, and adhesion properties upon switching the temperature from below to above the LCST while the permeability of redox probes through the film remains unchanged. The physicochemical properties of the microgel films could be explained assuming that during the assembly of PAH, diffusion of the polyelectrolyte chains into the microgel takes place, at least partially.

Polyelectrolytes could indeed diffuse into the microgel porous structure in addition to adsorbing on their surface. Diffusion of polyelectrolytes inside charged hydrogels will depend on the pore size of the microgel and on the charge of both the diffusing polyelectrolyte and the microgel. Since PAH is positively charged, it will face attractive interactions with P(NIPAm-*co*-MAA) microgels that would facilitate diffusion inside the pores, and complexation with MAA negative charges inside the hydrogel core. At the same time, the presence of charges on the surface of the hydrogel can lead to PAH complexation on the surface of the microgel, which may also lead to recharging and blocking of pores and finally prevent additional PAH chains from entering the microgel core. Interesting results about the interaction of temperature and pH-sensitive P(NIPAm-*co*-MAA) microgels with polyelectrolytes have been already reported.[18,19] P(NIPAm-*co*-MAA) microgels exposed to oppositely charged polyelectrolytes of different molecular weight showed different electrophoretic mobility and hydrodynamic radius depending on the molecular weight of the polyelectrolyte. Some authors postulated that the oppositely charged polyelectrolyte chains penetrate into the microgel structure,[20,21] while others suggested the accumulation of the polyelectrolytes on the microgel interface.[22] Whether the polyelectrolyte deposits on the microgel surface or penetrates the microgel has not been fully demonstrated. Dobrynin *et al.*[23] have demonstrated that the surface adsorption of polyelectrolytes on an oppositely charged surface depends on the surface charge density, the fraction of the charged monomers on the polyelectrolyte and the ionic strength.

Gelissen *et al.*[24] recently investigated a model core–shell PNIPAm-based microgel with a cationic core of *N*-(3-aminopropyl) methacrylamide hydrochloride and an anionic shell of monomethylitaconate to study whether the presence of a negatively charged shell shields the cationic core while still enabling the uptake and release of anionic guest polyelectrolytes. These microgels were loaded with polystyrene sulfonate of different molecular weights to study the influence of their chain length on polymer uptake and release. Using small-angle neutron scattering, the authors evaluated the spatial distribution of polystyrene sulfonate within the microgels and found that the location of polystyrene sulfonate in the microgel depends on the molecular weight of the polymer. In this work we aimed to advance understanding of the interaction of negatively charged PNIPAm microgels with positively charged PAH molecules. Our goal was to better understand how polyelectrolyte chains associate with the microgel and to determine how this association is affected by the temperature-induced collapse of PNIPAm chains, which leads to a redistribution of the charged moieties.

Experimental part

Materials

All purchased chemicals were used as received without further purification: *N*-isopropylacrylamide (NIPAm, Aldrich 97%), *N*,*N*′-methylene-bis-acrylamide (MBA, Aldrich 99%), ammonium persulfate (APS, Aldrich 98%), polyallylamine hydrochloride of 15 kDa (PAH 15 kDa, Aldrich), polyallylamine hydrochloride of 50 kDa (PAH 50 kDa, Aldrich), and polyallylamine hydrochloride of 140 kDa (PAH 140 kDa, Alfa Aesar). Methacrylic acid (MAA, Aldrich, 99%) was distilled before use.

Microgel synthesis and characterization

Synthesis. Microgel synthesis was performed according to Zavgorodnya *et al.*[25] 100 mL solution containing 12 mmol of NIPAm and 0.28 mmol of BIS in Milli Q water was heated up to 70 °C with magnetic stirring and purged with N_2 in a three neck 250 mL round-bottom flask for 1 h. After this time, 1.72 mmol of MAA was added to the polymerization solution and mixed for 10 min more. Finally, the reaction was initiated by adding 0.046 g of APS dissolved in 1 mL of Milli Q water at room temperature. After 4 h of reaction at 70 °C, the microgels were purified by centrifugation/re-suspension in water three times. Core–shell particles were prepared under the same conditions, except that the 1.72 mmol of MAA was added to the reaction 15 minutes after it started. ^{1}H-NMR spectra of both microgels and assignments of resonance signals are shown in Fig. S1 (ESI†).

Dynamic light scattering (DLS) measurements. The size and size distribution of the PNIPAm-based microgels were determined by dynamic light scattering (DLS) as a function of temperature using a Zetasizer Nano-ZS90 (Malvern Instruments Ltd). The experiments were performed with 1 mg ml^{-1} of microgel dispersions in 5 mM KCl exposed to increasing amounts of PAH of different molecular weights (15, 50, and 140 kDa) at 20 and 40 °C.

Confocal microscopy and flow cytometry determinations. Confocal microscopy imaging was performed with confocal microscope ZeissLSM 880 (Carl Zeiss Gmbh). Acquisition and analysis are controlled by Zen black software. The excitation wavelength was 488 nm of an argon laser and emission was collected using a GaASP detector coupled with transmission,

T-PTM. The objective used was a 100× EC Plan-Neofluar (oil, 1.3 NA) objective. The kinetic experiments were carried out acquiring 1024 × 1024 pixel frames with 10× digital zoom and 120 time series with a 1.2 s frame rate. The samples were stabilized for 10 minutes at different temperatures before time series acquisition using a temperature-controlled insert in the microscope stage.

The FACS experiment was performed with a BD FACSCanto II instrument. A PE channel (a 585/42 nm filter with a 556 nm long pass filter) was used to study the labelled PAH uptake inside the microgel. BD™ CS&T beads were run before the experiment to ensure the correct performance of the instrument. To determine the microgel population a non labelled microgel was tested in terms of the forward (FSC) and side scatter (SSC) characteristics. Microgels unlabeled and labelled with the maximum percentage of PAH were employed to fix the PE-A voltage. 10 000 events were acquired for each sample. FlowJo 7.5 software was used to analyze the data.

Isothermal titration calorimetry. ITC experiments were performed by using a MicroCal ITC200. The reference cell and sample cell of the calorimeter were loaded with Milli-Q water and 5 mM KCl aqueous microgel dispersion (1 mg ml^{-1}, 0.02 mM COOH units), respectively. The titrant syringe was filled with aqueous PAH solution (1.5 mM). For each experiment, 50 injections of 5 μL of PAH solution were done (with an initial injection of 1 μL, each at 2 s duration) at 900 s. Control experiments were performed by injecting identical volumes of buffer solution into the microgel dispersion and the aqueous PAH solution into the buffer solution, respectively. The reference power and the stirring speed were maintained at 5 μcal s^{-1} and 300 rpm throughout the experiment. The resulting corrected injection heats were plotted as a function of the molar ratio of PAH/microgel and fitted with the Origin software package provided with the ITC200 calorimeter. The experiments were performed at 20 °C and 40 °C. In the non-linear least squares fitting of the experimental data, the binding constant (K), the number of binding sites (N) and the standard molar enthalpy change (ΔH°) were obtained as adjustable parameters. From the values of K and ΔH°, the thermodynamic parameters standard Gibbs free energy change (ΔG°) and standard entropy change (ΔS°) were calculated according to the basic thermodynamic equation (eqn (1)):

$$\Delta G^\circ = -RT\ln K = \Delta H^\circ - T\Delta S^\circ \quad (1)$$

Results and discussion

Size and zeta potential changes. Molecular theory analysis

The synthetic protocols and the chemical characterization of the microgels are presented in the ESI.† The hydrodynamic diameter of the synthesized microgel particles changes when the particles are exposed to PAH below the LCST at 20 °C (Fig. 1A) and above the LCST at 40 °C (Fig. 1B). Experiments were performed with 1 mg ml^{-1} microgel dispersions in 5 mM KCl exposed to increasing amounts of PAH from a concentrated solution. The addition of PAH to the microgel solution was always performed at 20 °C. The mass of added PAH is represented as a percentage of the total microgel mass. PAH of different molecular weights (15, 50, and 140 kDa) was used. Table S1 (ESI†) shows the size and PDI values obtained.

Microgels not exposed to PAH displayed characteristic changes in size and zeta potential with temperature. Their diameter decreased from 1.2 μm to 0.24 μm when the temperature increased from 20 °C to 40 °C. As seen in Fig. 1A and Table S1 (ESI†), below the LCST, when PAH with a molecular weight of 15 kDa was added to 1 mg ml^{-1} microgel dispersion in 5 mM KCl, a compression of the hydrogel particles was observed up to a PAH concentration of 10%. This compression was followed by a linear increase in particle size at concentrations higher than 10%. Indeed, the particle size decreased from 1.2 μm to 0.8 μm in diameter from 0% to 10% PAH. Above 10% of PAH 15 kDa, the particle size increased slowly and linearly from 0.8 to 1.3 μm in diameter until 160% PAH. Above the LCST (40 °C) hydrogels with PAH 15 kDa show a hydrodynamic diameter from 0.24 μm to 0.55 μm when increasing the PAH concentration from 0 to 160%. Concentrations of PAH 15 kDa over 160% resulted in the destabilization of the hydrogel and subsequent precipitation.

In sharp contrast with the previous result, in the presence of PAHs with higher molecular weight a very different evolution of the microgel size was observed. The microgel exhibited a marked increase in size with 5% PAH of 50 kDa and 140 kDa both at 20 and at 40 °C, with more pronounced changes at 20 °C. This increase in size is probably indicative of aggregation. However, at 20 °C with the PAH concentration over 5% and up to 15% both MW resulted in a particle size comparable to the initial value, close to 1.2 μm. Over 15% PAH concentration, the particle size increased slowly and linearly from 1.0 to 1.4 μm in diameter with addition of PAH 50 kDa, up to 80% of PAH, and from 1.5 to 1.7 μm with the addition of PAH 140 kDa, up to 40% of PAH. Over the upper percentages of PAH, 80% for PAH 50 kDa and 40% for PAH 140 kDa, the microgel precipitates.

At 40 °C, the microgel with both PAH 50 and 140 kDa displayed a larger particle size than the naked microgel (0.24 μm). The differences in size with the microgel non complexed to PAH were more prominent for PAH 140 kDa than for PAH 50 kDa. In fact, after the initial large size values at 5%, probably due to microgel aggregation, the microgels displayed sizes of 1.4 μm for 15% of PAH 140 kDa and maintained that value until 40% PAH before precipitation. Similar behavior was observed in the case of PAH 50 kDa: at 40 °C for 15% PAH the particle size was 700 nm, remaining constant for PAH concentrations of up to 80% PAH, before precipitation.

These results evidence that the size and stability of P(NIPAm-*co*-MAA) microgels will be largely affected by the presence of PAH below and above the LCST and that the molecular weight of PAH plays a substantial role in the microgel behavior. In order to get more insight into the interaction of PAH with the microgels zeta potential measurements were performed. Fig. 2 illustrates the variations in zeta potential below and above the LCST for

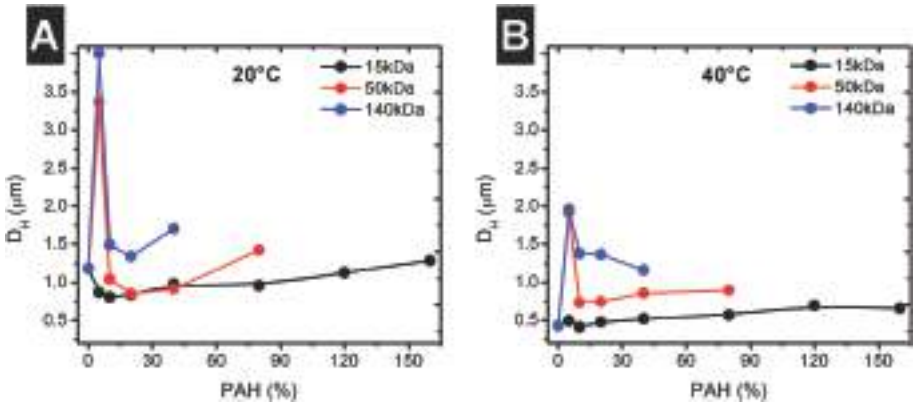

Fig. 1 Hydrodynamic diameter at 20 (A) and 40 °C (B) for P(NIPAm-*co*-MAA) microgels with increasing amounts of PAH of 15 kDa (black), 50 kDa (red), and 140 kDa (blue).

1 mg ml^{-1} microgel dispersions in 5 mM of KCl with an increasing amount of PAH with the three molecular weight studied: 15, 50, and 140 kDa.

The zeta potential values for the microgel without PAH at 20 °C were close to 0 mV, but decreased to −16 mV at 40 °C. This decrease in zeta potential can be attributed to the reduction in particle volume over the LCST, which favored the increase in charge density on the hydrogel surface. Additionally, charge segregation to the surface can occur, because the collapse of PNIPAm with temperature triggers its aggregation, forming a hydrophobic structure, which avoids the interaction of water by exposing the negatively charged MAA segments to the bulk. Such a rearrangement would also help in maintaining the colloidal stability of the microgel in aqueous media. We have previously reported this behavior for nanopillars based on PNIPAm and acrylamide.[26] Molecular modeling supports this approach as it will be explained below.

The 0 mV value of the microgel zeta potential at 20 °C was gradually increased with the addition of PAH 15 kDa, reaching a plateau close to +25 mV at 100% PAH, approximately. For PAH 50 kDa, the zeta potential at 20 °C also gradually increased with the addition of PAH, reaching +50 mV for 80% PAH without showing a clear plateau before destabilizing the system. On the contrary, the microgel-PAH 140 kDa system seemed to reach a plateau more steeply at around +48 mV with only 10% of polyelectrolyte.

Zeta potential measurements at 40 °C yielded the same profile as at 20 °C, but the plateau was reached with less PAH added in all cases. The microgel exposed to PAH 140 kDa reached the plateau with only 5% of PAH around +50 mV. For PAH 50 kDa, the plateau was clear with 10–15% of PAH, also around +50 mV. Finally, for PAH 15 kDa, the plateau was reached with 30–40% of polyelectrolyte, around +60 mV.

Based on the evolution of the microgel size and zeta potential with the concentration of PAH of different molecular weight, we can hypothesize that the low-molecular-weight polyelectrolyte can be incorporated inside the microgel with a high loading capacity, reaching up to 160%. The loading capacity of the microgel (the capacity of the microgel to associate with PAH without destabilizing and precipitating) decreases when the molecular weight of PAH increases, being 80% for PAH 50 kDa and only 40% for PAH 140 kDa. Based on the comparison of zeta potential values, we can argue that PAH accumulates more on the particle surface when its molecular weight increases, preventing its incorporation inside the microgel particle. Due to pore size considerations the penetration of

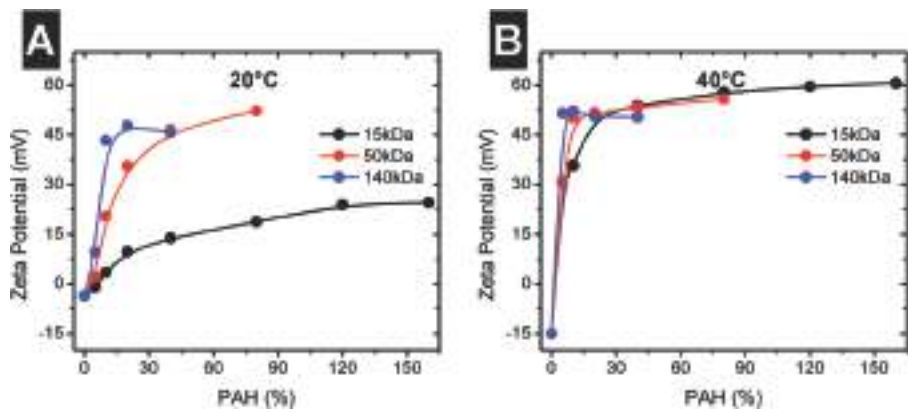

Fig. 2 Zeta potential changes at 20 (A) and 40 °C (B) for P(NIPAm-*co*-MAA) microgels with an increasing amount of PAH 15 kDa (black), 50 kDa (red), and 140 kDa (blue).

50 kDa PAH in the microgel is limited and even more the penetration of 140 kDa. Also, adding PAH with the highest molecular weight results in a plateau in the zeta potential at much lower amounts of PAH added, though yielding higher potential values due to overcompensation of charges in the microgel. Conversely, the low-molecular-weight PAH is able to penetrate the particle, compensating internal charges in the microgel. The large sizes observed at 5% PAH for 50 kDa and 140 kDa PAH evidence that PAH is depositing on the surface rather than being loaded inside the hydrogel and that at low concentrations PAH is not fully recharging the microgel surface, causing aggregation.

We have also applied molecular theory analysis to describe PAH adsorption to a P(NIPAm-*co*-MAA) network. Our goal was to investigate the subtle segregation of MAA units to the particle surface and explain the substantial increase of the microgel zeta potential up to −16 mV when the temperature increase. Also, understand the zeta potential values between +50 and +60 mV of the system, microgel-PAH, having the polyelectrolyte different molecular weights. The molecular theory approach followed is described in the ESI.† For the analysis we have considered a thin hydrogel film. Fig. 3 shows a schematic representation of the film, in which a random P(NIPAm-*co*-MAA) network grafted to a planar surface is in contact with an aqueous KCl solution containing 5 kDa PAH. Coordinate z corresponds to the distance from the supporting surface, placed at $z = 0$. We have studied this system above and below the LCST of PNIPAm. Fig. 3 also shows plots of the local volume fraction of network segments and PAH units as a function of the distance to the supporting surface. The upper panels show the NIPAm, MAA and deprotonated (charged) MAA profiles. The lower panels display the distribution of PAH segments. Two different temperatures are considered below (T = 20 °C; left-hand side panels) and above (T = 40 °C; right-hand side panels) the LCST of PNIPAm.

At a low T, the film extended up to $z \approx 130$ nm with both units, NIPAm and MAA, homogeneously distributed (see Fig. 3-A1). At this temperature, the low MW PAH partitioned homogeneously inside the film (see Fig. 3-A2). When the temperature increases above the LCST, the film thickness decreases to approximately 85 nm, with high accumulation of NIPAm segments at the top surface (see Fig. 3-B1). Because of the random structure of the network, this aggregation of NIPAm at the top surface led to a relatively high concentration of MAA in this region. Additionally, a higher density of charged MAA units occurred in this region of NIPAm aggregation. Consequently, PAH was adsorbed predominantly on the top surface of the film, showing a relatively high volume fraction in this region (see Fig. 3-B2). Under these conditions, PAH also partitioned inside the film, though to a lesser extent than on the surface. Our theoretical results for a hydrogel film grafted to a planar surface clearly show that MAA segregation towards the surface as the temperature increases above the LCST of NIPAM leads to surface adsorption. These results, however, do not attempt to capture the peculiarities of PAH adsorption to the microgels.

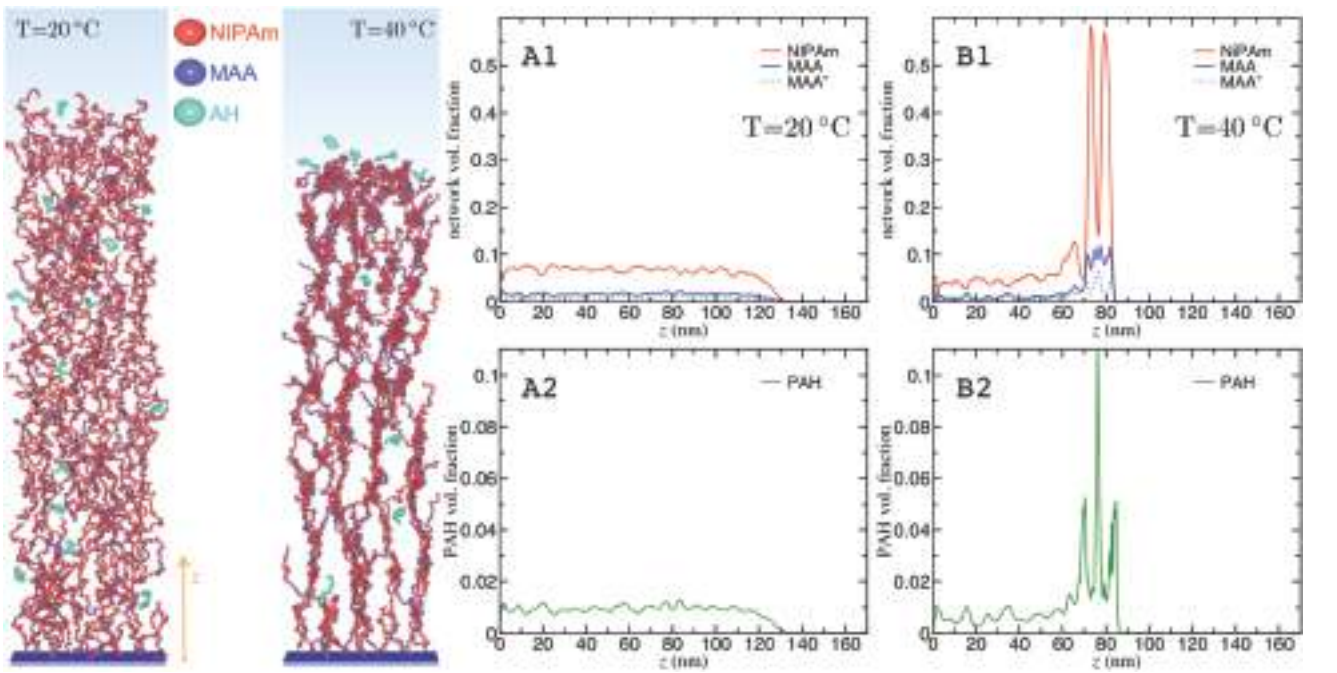

Fig. 3 Left: Scheme representing the system considered in our molecular theory study. A random P(NIPAm-*co*-MAA) network grafted to a planar surface is in contact with an aqueous solution containing PAH. Coordinate z measures the distance from the supporting surface that sits at $z = 0$. The panels show typical network configurations below (20 °C) and above (40 °C) the LCST of PNIPAm. Right: Plots of the local volume fraction of network segments and PAH units as a function of the distance to the supporting surface. The upper panels (A1 and B1) show the NIPAm and MAA as well as deprotonated (charged) MAA profiles; the lower panels (A2 and B2) display the distribution of PAH segments.

Rumyantsev *et al.*[27] have demonstrated similar results using a complex mean-field theory and computer simulations. These authors predict an equilibrium center-to-periphery mass redistribution in a microgel particle. The authors demonstrated the effect of high- and low-molecular-weight species for controlled encapsulation, transport, and release of high- and low-molecular-weight species in many processes.

Confocal microscopy and flow cytometry determination

To gain further insight into the location of PAH in the microgel, we exposed the microgels to fluorescently labelled PAH 15, 50 and 140 kDa and imagined them using confocal laser scanning microscopy (CLSM) (Fig. 4A and B) (see the ESI† for experimental details). From CLSM images we expected to discriminate if the PAH would locate on the surface of the hydrogel particles or distribute inside them. Fig. 4A illustrates a micrograph of the microgel with 30% of labelled PAH 50 kDa. This micrograph shows that the hydrogel particles lose volume to a larger extent than the changes in the hydrodynamic radii observed with DLS. Since the hydrogel displays sizes below 500 nm, it is not possible to determine the location of the labelled chains. A homogenous distribution of fluorescence in the particles in the presence of the labelled PAH is observed. Images taken at 20 and 40 °C did not show significant differences.

In order to confirm that the interaction between the microgel and PAH was restricted to the negatively charged methacrylyc acid group, core–shell microgels were prepared. Differently from the random co polymerization, in the core shell microgels the core was synthesized only with the NIPAm monomer while the NIPAm and MAA monomers were used for the shell (experimental details available in the ESI†). For the core–shell P(NIPAm-*co*-MAA) microgels (Fig. 4B), in the presence of labelled PAH the confocal image reveals a fluorescent shell around a dark core. This means that the labelled PAH was confined to the outer region of the hydrogel, confirming that PAH interacts with the charged MAA, which is only present in this region (Fig. 4B).

We performed flow cytometry studies for a more precise quantification of the PAH uptake by the microgels. Flow cytometry allows us to measure the fluorescence per hydrogel particle as a function of the concentration of labelled PAH in the bulk. In these experiments, the microgel was exposed to an increasing amount of labelled PAH 15 kDa and 50 kDa. Experiments were not performed with PAH 140 kDa to avoid instrumental problems, due to the low stability of the formed complexes and precipitation issues. Fig. 4C and D display the maximum intensity of the hydrogel dispersion depending on the increasing addition of PAH. Fluorescence intensity *vs.* particle number distribution is presented in the ESI.† For PAH 15 kDa (see Fig. 4D), the normalized intensity increased up to 30–35% of PAH addition in the microgel dispersion. Above 35%, the normalized intensity seemed to remain constant with the increase of PAH in the system. For PAH 50 kDa, the plateau was reached before, and the normalized intensity did not change above 10% of PAH.

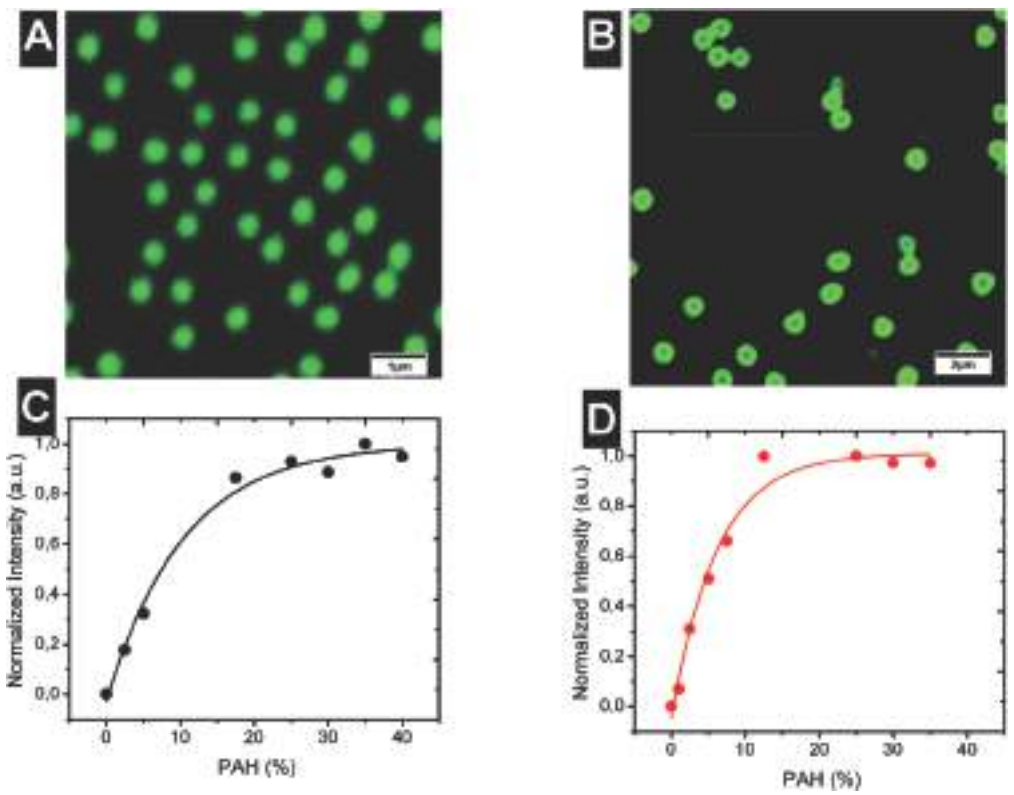

Fig. 4 Up: Confocal micrographs of statistical P(NIPAm-*co*-MAA) microgels (A) and core–shell P(NIPAm-*co*-MAA) microgels (B) with rhodamine-labelled PAH 15 kDa. Down: Maximum intensity of the hydrogel dispersion depending on the increasing addition of PAH of 15 kDa (C) and 50 kDa (D).

The flow cytometry data are in agreement with the zeta potential and DLS measurements and confirm that the 50 kDa PAH remains at least partially on the surface of the hydrogels, while PAH 15 kDa is able to accumulate inside. This difference in uptake between the two MW PAH is indicative of the large PAH chains being stopped by the pore sizes in the hydrogels. However, it cannot be concluded that for 50 kDa the chains are only located on the surface of the hydrogel. 50 kDa is an average weight, and there are smaller chains present that could get into the core. In addition, the interface of the hydrogel has fuzzy characteristics, and pores may change size from the surface to the inner core, so partial penetration of PAH chains could be possible.

Thermodynamic studies

In order to evaluate the thermodynamics of the interaction between PAH and P(NIPAm-*co*-MAA) microgels, isothermal titration calorimetry (ITC) studies were performed. ITC is a very sensitive technique that allows one to obtain the thermodynamic characteristics of associative processes in solution.[28] In this context, Fig. 5 shows the heat resulting from the titration of microgel dispersions with aliquots of 2 μL of PAH 15 kDa or PAH 50 kDa at 20 °C. Table 1 displays the thermodynamic parameters of each titration obtained after fitting. Two site fittings were demonstrated to be the best fitting conditions for our system.

Wang *et al.*[29] studied the binding of sodium dodecyl sulphate to PNIPAm microgels using ITC. The authors found an endothermic heat for binding events below the LCST, though above the LCST it became exothermic. In our case, the data obtained at 40 °C are not reported here as they could not be properly fitted (data not shown). Only experiments conducted at 20 °C will be reported. Fittings were performed applying two-site models, assuming that one site corresponds to the PAH incorporated into the microgel particle and the other to the PAH associated with the microgel surface.

Table 1 Binding constants (K_i), standard enthalpy changes (ΔH_i°), standard entropy changes ($T\Delta S_i^\circ$) and standard free energy changes (ΔG_i°) for the association between P(NIPAm-*co*-MAA) microgels and PAH with different molecular weights obtained from isothermal tritation calorimetry analysis at 20 °C

	μgel-PAH^{15kDa}	μgel-PAH^{50kDa}
Chi^2	99.67	141.0
10^{-5} K_1	1.5	9.4
N_1	0.7	0.01
ΔH_1° (kJ mol^{-1})	1.0	46.0
ΔS_1° (kJ mol^{-1})	0.10	0.27
ΔG_1° (kJ mol^{-1})	−29.0	−34.3
10^{-5} K_2	0.21	0.90
N_2	1.8	2
ΔH_2° (kJ mol^{-1})	−1.71	−1.49
ΔS_2° (kJ mol^{-1})	0.08	0.09
ΔG_2° (kJ mol^{-1})	−24.2	−27.9

For site 1, PAH incorporated into the microgel, the highest association constant K_1 for PAH 50 kDa was found to be 6 times higher than for PAH 15 kDa. However, the number of association points (N_1) was only 0.01 for PAH 50 kDa, while for PAH 15 kDa this number was 0.7. As regards PAH associated with the particle surface, PAH 50 kDa yielded the highest association constant K_2, 4.5 times higher than for PAH 15 kDa. Moreover, the number of association points was 0.9 for PAH 50 kDa and 0.21 for PAH 15 kDa, 4 times higher for the former.

For site 1, corresponding to interactions within the hydrogel, the heat was endothermic for both PAH 15 kDa and 50 kDa. However, for PAH 15 kDa, the endothermic heat measured was 1 kJ while for 50 kDa it was 46 kJ. Since the interaction between

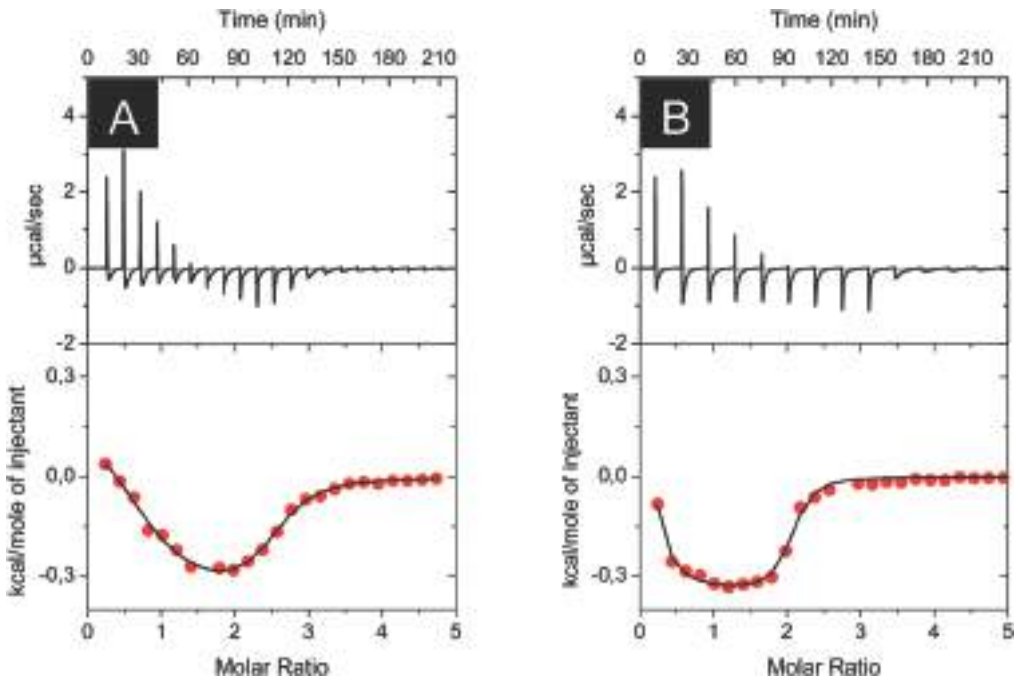

Fig. 5 ITC titration curves of microgel-PAH$^{15\,000}$ (A) and microgel-PAH$^{50\,000}$ (B) at 20 °C using aliquots of 2 μL.

oppositely charged polymers is usually exothermic, the endothermic heat can be understood as the dehydration and breakage of hydrogen bonds, mainly from carboxylate groups of MAA, which are highly hydrated. The significantly lower endothermic heat for PAH 15 kDa is due to a larger gain through electrostatic interactions when the polymer is smaller. Probably, larger PAHs can interact with fewer carboxylate groups than the smaller chains, which can place themselves more easily inside the pore structure and arrange for better interaction. In previous work, we demonstrated that hydrogen bonds can be formed between the carboxylates of PMAA and NIPAm groups.[30] In this context, aside from the dehydration and rupture of the hydrogen bonds of the carboxylates with water, the endothermic heat may also result from the rupture of these hydrogen bonds when PAH is interacting with the carboxylate groups. The endothermic heat must be compensated by an increase in entropy that favors the interaction between PAH and the hydrogel. There are several possible contributions to an increase in entropy. First, counterions from PAH and MAA can be released through the interaction with the microgel as the negative charges from MAA compensate at least partially the positively charged amines from PAH. The release of counterions increases the number of free species, *i.e.* one ion for each monomer involved. There is also a loss in water structure as the PAH interacts with carboxylate groups, since water associated with PAH and MAA is released through the interaction between the polymers. The rupture of hydrogen bonds between NIPAm and carboxylates could be interpreted as an increase in entropy, since the linkage between the monomer of PNIPAm and the carboxylates would be broken and give more rotational freedom to both monomers. On the other hand, there are several processes leading to a decrease in entropy: the binding of PAH chains to the hydrogel results in a loss of freedom for the polymer as a freely diffusing polymer chain and the association of the carboxylates to the charged amines of PAH should restrict conformational freedom for both groups.

With regard to site 2, PAH interacting with carboxylate groups on the surface of the hydrogel, the heat is exothermic. The exothermic heat comes from the electrostatic interaction between positively charged amines in PAH and negatively charged carboxylates in MAA, which is larger in this case than the endothermic heat from the dehydration and rupture of hydrogen bonds associated with MAA. This can be understood in the light of the PAH chains deposited on the surface of the hydrogel, which find it easier to arrange in such a way that the interaction between carboxylates and amines is maximized. Entropy also contributes positively, though to a lesser extent than in site 1. This may be explained by a smaller number of carboxylates and PAH molecules associated with site 2. We have seen that, at least for PAH 15 kDa, most of the polymer seems to be in the hydrogel core. For PAH 50 kDa, despite the fact that most polymers are on the surface, their presence inside the hydrogel cannot be ruled out. Moreover, it is also possible that a significant number of PAH 50 kDa monomers may not interact with inner carboxylate groups when placed on the surface, and consequently the number of counterions released may be small.

The ITC results are in line with our DLS and zeta potential results at 20 °C. The zeta potential values are less positive for PAH 15 kDa, evidencing higher incorporation of the polymer inside the microgel particle, as it has been also demonstrated by flow cytometry. On the other hand, the increase in zeta potential to a 20 mV value with PAH 50 kDa evidences more accumulation of the polymer on the surface and a large number of non-compensated amine groups.

Truzzolillo *et al.*[31] investigated the complexation of thermoresponsive anionic PNIPAm microgels and cationic ε-polylysine (ε-PLL) chains. They proposed that short PLL chains adsorb onto microgels and act as electrostatic glue above the LCST. Our results suggest a different scenario, with a high incorporation of the polymer inside the microgel particle for short chains of PAH. Considering the characteristics of the microgels obtained by the authors, our microgels display more charged groups, which can induce a higher electrostatic interaction with PAH and promote the incorporation of short polymer chains inside the microgel.

Release of doxorubicin from the microgel in the presence of PAH

Various microgel systems have been used to load and release bioactive molecules.[6,32] In this context, and to gain insight into the availability of carboxylate groups in the microgel for complexation of small molecules, prior to the interaction with PAH we loaded the microgels with positively charged drugs and then exposed them to PAH. Since the microgels could be used for transport of positive drugs and cancer cells secrete polyamines as by-products, we chose as a model drug doxorubicin (DOX), which is a positively charged carcinogenic drug, being also fluorescent.

Fig. 6A shows the variations in fluorescence emission at 488 nm, the wavelength of maximum intensity, exciting at 295 nm (see the fluorescence spectra in the ESI†) as a function of time at 20 °C of microgels pre-loaded with doxorubicin after addition of 5 and 40% of PAH 15 kDa and 140 kDa. The fluorescence intensity decreased after addition of PAH 15 kDa. Independently of the concentration of PAH the fluorescence intensity of the microgels loaded with DOX reaches its minimum after 5 seconds. Instead, the changes in fluorescence intensity after the addition of PAH 140 kDa revealed a slower replacement of DOX, more dependent on the PAH concentration. For 5% of PAH, the fluorescence intensity decreases to 35% 10 seconds after PAH addition. But, for 40% PAH 140 kDa, the fluorescence intensity decreased to 20% after 6–8 seconds of exposure to the polymer. The differences observed in the decrease in fluorescence depending on the PAH molecular weight and concentration hint at different kinetics in the release of pre-loaded doxorubicin in the microgel. Fig. 6b shows the confocal micrographs of the microgel pre-loaded with doxorubicin at different exposure times, 0, 5, 7 and 20 seconds to 5 and 40% of PAH 15 kDa and 140 kDa. For 5% PAH of 140 kDa, the hydrogels still showed fluorescence 7 seconds after the addition of the polymer. It is likely that in this case the penetration of PAH 140 kDa inside the microgel is limited but then increases as the polymer concentration increases. It is worth highlighting that the decrease in intensity is not homogeneous among all microgels.

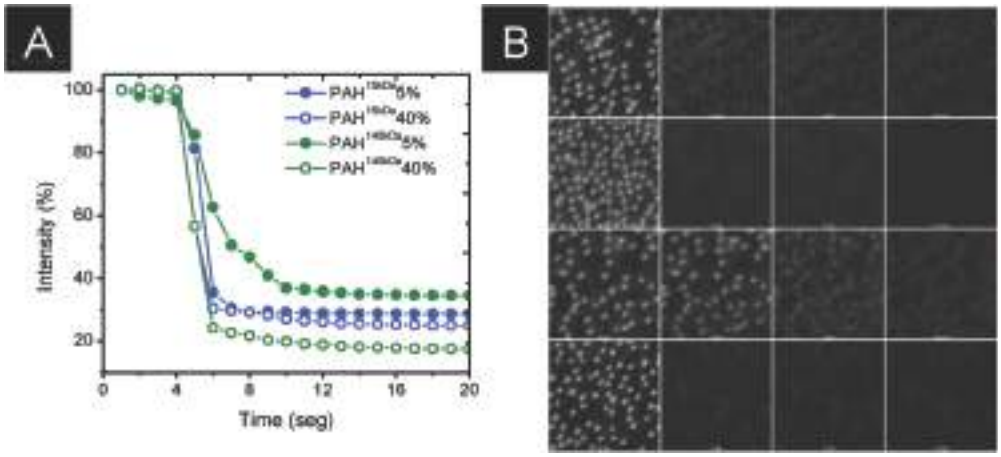

Fig. 6 Variation in fluorescence emission of hydrogels as a function of the exposure time to PAH at 20 °C with excitation at 295 nm of microgels pre-loaded with doxorubicin *in situ* contact with 5 and 40% of PAH 15 kDa and 140 kDa. (A) Fluorescence emission at the wavelength of maximum intensity as a function of time and (B) confocal micrographs of the microgel pre-loaded with doxorubicin at different exposure times, 0, 5, 7 and 20 seconds. Lines from top to bottom: PAH 15 kDa 5%, PAH 15 kDa 40%, PAH 140 kDa 5%, and PAH 140 kDa 40%.

We can conclude that PAH is very effective at expelling doxorubicin from the inside of the microgel particle, removing practically all doxorubicin in a short time. The low molecular weight PAH, 15 kDa, which we have shown to accumulate inside the microgel, results in an immediate release of doxorubicin at 5% PAH. At 40% the decrease seems faster, but the differences are not significant. 5% PAH 15 kDa is enough to remove most DOX, meaning that most carboxylate groups from the hydrogel are interacting with the amines from PAH. PAH 140 kDa remains mostly on the surface of the microgel as we have proved before. However, DOX in the interior of the microgel is removed but more slowly and the remaining fluorescence is higher. This hints that some polymer chains are entering the hydrogel but more slowly. At 40% the decrease in fluorescence is more effective and faster, meaning that there are more chains available to enter in the microgel and replace doxorubicin molecules.

Here, we have shown that P(NIPAm-*co*-MAA) microgels and PAH chains interact in a complex way, which depends on both the molecular weight of the polymer and temperature. Above NIPAm's LCST, PAH for all molecular weights studied will preferentially relocate on the microgel surface. Theoretical results predict this behavior even for low molecular weight PAH molecules and are confirmed experimentally by the highly positive zeta potential observed when the microgel is in contact with 15 kDa PAH solutions, while it is significantly lower at temperatures below the LCST as PAH diffuses in the microgel. Moreover, the small difference in size between the naked microgel and the microgel with small amounts of 15 kDa PAH suggests that the polymer accumulates on the surface without disturbing the microgel network. Increasing the PAH concentration leads to a slight increase in microgel size, which is likely to accumulate more polymer on the surface as confirmed by the increase in zeta potential. At 40 °C, the microgels exposed to 50 kDa PAH display similar behavior, only the microgel size is larger in agreement with the larger size of PAH. The presence of PAH on the surface of the microgel is a result of the segregation of charges of MAA on the surface of the microgel and the formation of a hydrophobic core inside following the LCST. The arrangement of the charges in the microgel is determinant for the location of the PAH. We have seen that core shell microgels with a PNIPAM core and a shell of NIPAM-MAA preferentially accumulate PAH on the surface below the LCST.

Below NIPAm's LCST the microgel response is more complex. Our results support the accumulation of 15 kDa PAH inside the particle network. PAH uptake inside the hydrogel occurs at low PAH concentrations; the size increase following the increase in PAH concentration implies that the PAH starts to deposit on the microgel surface as well. PAH accumulation inside the microgel is also hinted at by both the lower zeta potential and the different size compared to 40 °C as well as by calorimetry results, which show a large number of association points for PAH inside the microgel. For 140 kDa PAH the differences in size and zeta potential between 20 and 40 degrees are smaller, suggesting that the dominant process is always PAH adsorption on the microgel surface. At this temperature, 50 kDa PAH represents an intermediate case as the size and zeta potential results suggest that surface adsorption and incorporation inside the particle may be both taking place. Calorimetry studies, however, show a significantly lower amount of association points in the microgel core as compared to 15 kDa PAH, and surface adsorption is predominant.

Experiments with DOX loaded microgels show that the presence of PAH independently of its MW causes the displacement of encapsulated DOX, meaning that most of the carboxylate groups in the hydrogel are interacting with the polymer. This result confirms that even for 140 kDa PAH polymer chains get inside the hydrogel matrix.

Conclusions

The interaction of P(NIPAm-*co*-MAA) microgels with poly allyl amine hydrochloride is largely dependent on the molecular

weight of the polyelectrolyte, *i.e.* on the size of polymer chains. We observed different trends in the size and zeta potential of hydrogels in the presence of PAH, which suggest that at 20 °C there is accumulation of PAH inside the hydrogel for PAH of low MW, 15 kDa, and deposition of PAH on top of the hydrogel surface for high MW, 50 and 140 kDa. The interaction between the microgel and PAH is also largely affected by the LCST, above which there is accumulation of negative charges on the microgel surface. Above the LCST the partial segregation of the MAA moieties to the surface leads to PAH accumulation on the surface of the hydrogel for all MWs of PAH considered. Molecular modelling, confocal microscopy, flow cytometry and isothermal titration calorimetry support these conclusions. PAH molecules preferentially replace doxorubicin complexed to the MAA inside the microgel. Though the kinetics and extent of removal of doxorubicin will depend on the molecular weight and concentration of PAH the phenomenon can be observed for all MW and concentrations of PAH employed. This observation implies that for PAH 140 kDa there is partial penetration of the polymer chains in the microgel.

This work sheds light on the complexity of the interaction of microgels with polyelectrolytes. Our results provide understanding of the physicochemical processes that govern microgels, which can lead to their improved design.

Conflicts of interest

There are no conflicts to declare.

Acknowledgements

We thank the MAT2017-88752-R Retos project from the Ministerio de Economia, Industria y Competitividad, gobierno de España for support. This work was performed under the Maria de Maeztu Units of Excellence Program from the Spanish State Research Agency – Grant No. MDM-2017-0720. We also thank Dr. Julia Cope for her revision of the manuscript. J. M. G., A. I., N. A. P.-C., L. C., G. S. L. and O. A. acknowledge the financial support from the Consejo Nacional de Investigaciones Científicas y Técnicas, the Agencia Nacional de Promoción Científica y Tecnológica (PICT-2015-0346, PICT-2017-3515) and the Universidad Nacional de La Plata (PPID-2018-X027).

References

1 R. a. Álvarez-Puebla, R. Contreras-Cáceres, I. Pastoriza-Santos, J. Pérez-Juste and L. M. Liz-Marzán, *Angew. Chem., Int. Ed.*, 2009, **48**, 138–143.
2 K. C. C. Johnson, F. Mendez and M. J. Serpe, *Anal. Chim. Acta*, 2012, **739**, 83–88.
3 B. R. Saunders, N. Laajam, E. Daly, S. Teow, X. Hu and R. Stepto, *Adv. Colloid Interface Sci.*, 2009, **147–148**, 251–262.
4 J. Ramos, A. Imaz, J. Callejas-Fernández, L. Barbosa-Barros, J. Estelrich, M. Quesada-Pérez and J. Forcada, *Soft Matter*, 2011, **7**, 5067–5082.
5 M. K. Nguyen and E. Alsberg, *Prog. Polym. Sci.*, 2014, **39**, 1235–1265.
6 M. J. Serpe, K. a. Yarmey, C. M. Nolan and L. A. Lyon, *Biomacromolecules*, 2005, **6**, 408–413.
7 S. Seiffert, *J. Polym. Sci., Part A: Polym. Chem.*, 2014, **52**, 435–449.
8 S. Schmidt, T. Liu, S. Rütten, K. H. Phan, M. Möller and W. Richtering, *Langmuir*, 2011, **27**, 9801–9806.
9 B. Brugger and W. Richtering, *Langmuir*, 2008, **24**, 7769–7777.
10 M. J. Serpe, C. D. Jones and L. A. Lyon, *Langmuir*, 2003, **19**, 8759–8764.
11 L. A. Lyon, Z. Meng, N. Singh, C. D. Sorrell and A. John St, *Chem. Soc. Rev.*, 2009, **38**, 865–874.
12 M. W. Spears, E. S. Herman, J. C. Gaulding and L. A. Lyon, *Langmuir*, 2014, **30**, 6314–6323.
13 W. Xiong, X. Gao, Y. Zhao, H. Xu and X. Yang, *Colloids Surf., B*, 2011, **84**, 103–110.
14 J. E. Wong, A. M. Díez-Pascual and W. Richtering, *Macromolecules*, 2009, **42**, 1229–1238.
15 A. P. H. Gelissen, A. J. Schmid, F. A. Plamper, D. V. Pergushov and W. Richtering, *Polym.*, 2014, **55**, 1991–1999.
16 W. Xu, A. A. Rudov, R. Schroeder, I. V. Portnov, W. Richtering, I. I. Potemkin and A. Pich, *Biomacromolecules*, 2019, **20**, 1578–1591.
17 E. Maza, C. Von Bilderling, M. L. Cortez, G. Díaz, M. Bianchi, L. I. Pietrasanta, J. M. Giussi and O. Azzaroni, *Langmuir*, 2018, **34**, 3711–3719.
18 J. Kleinen and W. Richtering, *J. Phys. Chem. B*, 2011, **115**, 3804–3810.
19 S. Walta, D. V. Pergushov, A. Oppermann, A. A. Steinschulte, K. Geisel, L. V. Sigolaeva, F. A. Plamper, D. Wöll and W. Richtering, *Polym.*, 2017, **119**, 50–58.
20 M. R. Islam and M. J. Serpe, *Chem. Commun.*, 2013, **49**, 2646–2648.
21 M. R. Islam and M. J. Serpe, *Macromolecules*, 2013, **46**, 1599–1606.
22 E. Costa, M. M. Lloyd, C. Chopko, A. Aguiar-Ricardo and P. T. Hammond, *Langmuir*, 2012, **28**, 10082–10090.
23 A. V. Dobrynin and M. Rubinstein, *Macromolecules*, 2002, **35**, 2754–2768.
24 A. P. H. Gelissen, A. Scotti, S. K. Turnhoff, C. Janssen, A. Radulescu, A. Pich, A. A. Rudov, I. I. Potemkin and W. Richtering, *Soft Matter*, 2018, **14**, 4287–4299.
25 O. Zavgorodnya and M. J. Serpe, *Colloid Polym. Sci.*, 2011, **289**, 591–602.
26 B. Sanz, C. von Bilderling, J. S. Tuninetti, L. Pietrasanta, C. Mijangos, G. S. Longo, O. Azzaroni and J. M. Giussi, *Soft Matter*, 2017, **13**, 2453–2464.
27 A. M. Rumyantsev, A. A. Rudov and I. I. Potemkin, *J. Chem. Phys.*, 2015, **142**, 171105.
28 R. J. Falconer, *J. Mol. Recognit.*, 2016, **29**, 504–515.
29 G. Wang, R. Pelton and J. Zhang, *Colloids Surf., A*, 1999, **153**, 335–340.
30 J. M. Giussi, M. I. Velasco, G. S. Longo, R. H. Acosta and O. Azzaroni, *Soft Matter*, 2015, **11**, 8879–8886.
31 D. Truzzolillo, S. Sennato, S. Sarti, S. Casciardi, C. Bazzoni and F. Bordi, *Soft Matter*, 2018, **14**, 4110–4125.
32 C. M. Nolan, M. J. Serpe and L. A. Lyon, *Biomacromolecules*, 2004, **5**, 1940–1946.

